Estimating spatially distributed soil water content at small watershed scales based on decomposition of temporal anomaly and time stability analysis

Wei Hu[2,3] and Bingcheng Si[1,2]

[1]College of Hydraulic and Architectural Engineering, Northwest A&F University, Yangling, 712100, China

[2]University of Saskatchewan, Department of Soil Science, Saskatoon, SK S7N 5A8, Canada

[3]New Zealand Institute for Plant & Food Research Limited, Private Bag 4704, Christchurch 8140, New Zealand

Correspondence to: Bingcheng Si (bing.si@usask.ca)

Abstract

Soil water content (SWC) is crucial to rainfall-runoff response at the watershed scale. A model was used to decompose the spatiotemporal SWC into a time-stable pattern (i.e, temporal mean), a space-invariant temporal anomaly, and a space-variant temporal anomaly. The space-variant temporal anomaly was further decomposed using the empirical orthogonal function (EOF) for estimating spatially distributed SWC. This model was compared to a previous model that decomposes the spatiotemporal SWC into a spatial mean and a spatial anomaly, with the latter being further decomposed using the EOF. These two models are termed temporal anomaly (TA) model and spatial anomaly (SA) model, respectively. We aimed to test the hypothesis that underlying (i.e., time-invariant) spatial patterns exist in the

space-variant temporal anomaly at the small watershed scale, and to examine the advantages of the TA model over the SA model in terms of the estimation of spatially distributed SWC. For this purpose, a dataset of near surface (0–0.2 m) and root zone (0–1.0 m) SWC, at a small watershed scale in the Canadian prairies, was analyzed. Results showed that underlying spatial patterns exist in the space-variant temporal anomaly because of the permanent controls of "static" factors such as depth to the $CaCO_3$ layer and organic carbon content. Combined with time stability analysis, the TA model improved the estimation of spatially distributed SWC over the SA model, especially for dry conditions. Further application of these two models demonstrated that the TA model outperformed the SA model at a hillslope in the Chinese Loess Plateau, but the performance of these two models in the GENCAI network (~250 km^2) in Italy was equivalent. The TA model can be used to construct a high-resolution distribution of SWC at small watershed scales from coarse-resolution remotely sensed SWC products.

Keywords: Soil moisture; Soil water downscaling; Empirical orthogonal function; Statistical models; Time stability

1. Introduction

Soil water content (SWC) of surface soils exerts a major influence on a series of hydrological processes such as runoff and infiltration (Famiglietti et al., 1998; Vereecken et al., 2007; She et al., 2013a). Soil water content in the root zone is, in many cases, linked to vegetative growth (Wang et al., 2012; Ward et al., 2012; Jia and

43 Shao, 2013). Obtaining accurate information on the spatiotemporal SWC is crucial for
44 improving hydrological prediction and soil water management (Venkatesh et al., 2011;
45 Champagne et al., 2012; She et al., 2013b; Zhao et al., 2013). While remote sensing
46 has advanced SWC measurements of surface soils (<5 cm in depth) at basin
47 (2,500–25,000 km^2) and continental scales (Robinson et al., 2008), characterization of
48 spatially distributed SWC at small watershed (0.1–80 km^2) scales still poses a
49 challenge. A method is needed for estimating spatially distributed SWC in the near
50 surface and root zone at watershed scales.

51 Time stability of SWC, which refers to similar spatial patterns of SWC across
52 different measurement times (Vachaud et al., 1985; Brocca et al., 2009), has been used
53 for estimating spatially distributed SWC (Starr, 2005; Perry and Niemann, 2007;
54 Blöschl et al., 2009). This method is conceptually-appealing, but assumes completely
55 time-stable spatial patterns of SWC.

56 The time-stable pattern does not explain all of the spatial variances in SWC,
57 indicating the existence of time-variant components (Starr, 2005). In order to identify
58 underlying patterns of SWC that have time-variant components, the spatiotemporal
59 SWC was decomposed into a spatial mean and a spatial anomaly. The spatial anomaly
60 of the SWC was further decomposed into the sum of the product of time-invariant
61 spatial patterns (EOFs) and temporally varying, but spatially constant coefficients
62 (ECs) using the empirical orthogonal function (EOF) (Fig. 1) (Jawson and Niemann,
63 2007; Perry and Niemann, 2007, 2008; Joshi and Mohanty, 2010; Korres et al., 2010;
64 Busch et al., 2012). Spatially distributed SWC estimates based on the decomposition

of spatial anomaly outperformed those based on time-stable patterns (Perry and Niemann, 2007).

Recently, the spatiotemporal SWC was also decomposed into a temporal mean and a temporal anomaly (Mittelbach and Seneviratne, 2012) (Fig. 1). Previous studies indicated that the contribution of the temporal anomaly to the total spatial variance was notable (Mittelbach and Seneviratne, 2012; Brocca et al., 2014; Rötzer et al., 2015). These studies, however, only focused on surface soils at large scales (> 250 km^2). Vanderlinden et al. (2012) suggested that the temporal mean may be further decomposed into its spatial mean and residuals, and the temporal anomaly may be further decomposed into space-invariant term (i.e., spatial mean of temporal anomaly) and space-variant term (i.e., spatial residuals of temporal anomaly) (Fig. 1). Note that the spatial variance in the temporal anomaly (Mittelbach and Seneviratne, 2012) equals that of the space-variant term of the temporal anomaly (Vanderlinden et al., 2012). The further decomposition of the temporal anomaly may be physically meaningful, because the space-invariant and space-variant terms in the temporal anomaly may be forced differently. However, the models of Mittelbach and Seneviratne (2012) and Vanderlinden et al. (2012) have not been used for estimating spatially distributed SWC. If the space-variant terms are ignored during the estimation of spatially distributed SWC, their models are equivalent to that based on time-stable patterns. Therefore, estimation of spatially distributed SWC may be improved by incorporating the space-variant term of the temporal anomaly if underlying (i.e., time-invariant) spatial patterns exist in the temporal anomaly.

To our knowledge, the importance of the space-variant term of the temporal anomaly and its physical meaning at small watershed scales is not well-known. Based on previous studies (Perry and Niemann, 2007; Mittelbach and Seneviratne, 2012; Vanderlinden et al., 2012), we assume soil water dynamics at watershed scales can be decomposed into three components (Fig. 1): (1) time-stable pattern (i.e., temporal mean, spatial forcing): the "static" factors such as soil and topography control the pattern; (2) space-invariant temporal anomaly (temporal forcing): the "dynamic" factors such as meteorological variables and vegetation change with time, and therefore modify SWC in time, regardless of spatial locations; and (3) space-variant temporal anomaly (interactions between spatial forcing and temporal forcing): this term represents interactions between "static" and "dynamic" factors. For example, SWC recharge introduced by a rainfall may be modified by topography through runoff processes; SWC loss triggered by evapotranspiration may be regulated by topography through solar radiation exposure.

The "static" factors may be persistent in the space-variant temporal anomaly, and their impacts on the space-variant temporal anomaly likely change with time. Thus, we hypothesize that some underlying (i.e., time-invariant) spatial patterns exist in the space-variant temporal anomaly, and their impacts can be modulated by a time coefficient, both of which can be obtained by the EOF method (Fig. 1). If the hypothesis is true, the estimation of spatially distributed SWC utilizing the EOF decomposition may outperform the one suggested by Perry and Niemann (2007). This is because: (1) the spatial anomaly which was decomposed using the EOF in Perry

and Niemann (2007) lumped the time-stable pattern and space-variant temporal anomaly together (Fig. 1); (2) the underlying spatial patterns in the spatial anomaly may not fully capture both time-stable patterns and patterns in the space-variant temporal anomaly due to the possible nonlinear relations between these two terms.

Therefore, the objectives were (1) to test the hypothesis that underlying spatial patterns exist in the space-variant temporal anomaly at small watershed scales and (2) to examine whether the decomposition of the space-variant temporal anomaly using the EOF has any advantages over the decomposition of the spatial anomaly (Perry and Niemann, 2007) for estimating spatially distributed SWC. Two steps were included in the estimation of spatially distributed SWC. First, the spatial mean SWC was upscaled from the SWC measurement at the most time-stable location using time stability analysis. Following this, the spatially distributed SWC was downscaled from the estimated spatial mean SWC. For the purpose of this study, spatiotemporal SWC datasets at depths of near surface (0–0.2 m) and root zone (0–1.0 m) from a Canadian prairie landscape were used. Spatiotemporal SWC of samples taken 0–0.06 m from a hillslope (100 m) in the Chinese Loess Plateau and 0–0.15 m from the GENCAI network (~250 km^2) in Italy were also used to further demonstrate conditions under which the decomposition of the spatial anomaly was beneficial to the estimation of spatially distributed SWC.

2. Materials and methods

2.1 Study area and data collection

This study was mainly conducted in the Canadian prairie pothole region (hereafter abbreviated as Canadian site) at St. Denis National Wildlife Area (52°12′ N, 106°50′ W) with an area of 3.6 km^2. This area has a humid continental climate (Peel et al., 2007), and had a mean annual air temperature of 1.9 ℃ and a mean annual precipitation of 402 mm during the study period (Fig. 2). A variety of depressions, knolls, and knobs result in a sequence of undulating slopes (Biswas et al., 2011). The elevation varies from 554.8 to 557.5 m. The soils are dominated by clay loam textured Mollisols (Soil Survey Staff, 2010) and covered by mixed grass, i.e., smooth brome grass (*Bromus inermis*) and alfalfa (*Medicago sativa* L.). The near surface soil porosity ranges from 38% (knolls) to 70% (depressions). Calcium carbonates ($CaCO_3$) derived mostly from fragments of limestone rocks are common in the Canadian Prairies. The $CaCO_3$ is dissolved by the slightly acidic rainwater moving through the upper horizons and deposited to lower horizons. The heterogeneous amount of infiltrated water resulted in a varying depth of $CaCO_3$ layer ranging from almost 0 m in the knolls to 2.1 m in the depressions. A 576 m long sampling transect with 128 sampling locations spaced at 4.5 m intervals was established over several rounded knolls and depressions. At each location, a time domain reflectometry probe was used to measure SWC of the near surface soil (0–0.2 m), and a neutron probe was used to collect SWC measurements at 0.2 m intervals between a depth of 0.2 and 1.0 m. The SWC was measured on a volumetric basis and expressed as a percentage (%) volume of water per unit soil volume. The SWC of the root zone was calculated by averaging the SWC of 0–0.2, 0.2–0.4, 0.4–0.6, 0.6–0.8, and 0.8–1.0 m. Soil water content was

152 measured on 23 dates from July 17, 2007 to September 29, 2011. The SWC dataset
153 was collected in all seasons except winter, and accurately portrays the variations in
154 soil water conditions in the study area. In addition to the SWC dataset, the soil,
155 vegetative, and topographical properties were obtained at each sampling location.
156 These properties included soil particle components (clay, silt, and sand contents), bulk
157 density, soil organic carbon (SOC) content for the surface layer, A horizon depth, C
158 horizon depth, depth to the $CaCO_3$ layer, leaf area index, elevation, cos(aspect), slope,
159 curvature, gradient, upslope length, solar radiation, specific contributing area,
160 convergence index, wetness index, and flow connectivity. Detailed information on the
161 measurements can be found in Biswas et al. (2012). The datasets from the Canadian
162 site were used to demonstrate the following two aspects in detail: (1) different
163 components of spatiotemporal SWC and their contributing factors, and (2) the
164 advantages of the new decomposition method over the method suggested by Perry and
165 Niemann (2007) in terms of the estimation of spatially distributed SWC.
166 To further test the applicability of the new method, we compared its performance at
167 two other sites, covering both the hillslope and the large watershed scale. Along a
168 hillslope of 100 m in length in the Chinese Loess Plateau, SWC of 0–0.06 m was
169 measured 136 times from June 25, 2007 to August 30, 2008 by a Delta-T Devices
170 Theta probe (ML2x) at 51 locations (Hu et al., 2011). The hillslope was covered by
171 *Stipa bungeana* Trin. and *Medicago sativa* L. in sandy loam and silt loam soils. In the
172 GENCAI network (~250 km^2) in Italy, SWC of 0–0.15 m was measured by a TDR
173 probe at 46 locations, 34 times from February to December in 2009 (Brocca et al.,

2012, 2013). The GENCAI area was dominated by grassland with a flat topography, in silty clay soils.

2.2 Statistical models for decomposing soil water content

Spatiotemporal SWC at small watershed scales was decomposed into three components: time-stable pattern, space-invariant temporal anomaly, and space-variant temporal anomaly. This model was compared to the one that decomposed SWC into spatial mean and spatial anomaly (Perry and Niemann, 2007). Both the space-variant temporal anomaly and spatial anomaly were decomposed using the EOF method. The two models are termed temporal anomaly (TA) model and spatial anomaly (SA) model, respectively. Figure 1 displays the differences between the two models. Each component will be explained in detail later. The explanation of nomenclatures is listed in Table A1. Because we focus on estimating spatial distribution of SWC at any given time, only spatial variances of SWC were taken into account. Therefore, the variance or covariance denotes the quantity in space without specifications.

2.2.1 The SA model

Perry and Niemann (2007) expressed SWC at location *n* and time *t* (S_{tn}) as (Fig. 1):

$$S_{tn} = S_{t\hat{n}} + Z_{tn}, \qquad (1)$$

where $S_{t\hat{n}}$ is the spatial mean SWC at time *t* (temporal forcing) and Z_{tn} is the spatial anomaly of SWC (lumped spatial forcing and interactions). The subscript $\hat{n}$ ($\hat{t}$) indicates a space (time) averaged quantity.

According to Perry and Niemann (2007), $S_{t\hat{n}}$ can be estimated by remote sensing, water balance models, and in situ soil water measurement at a representative (or

time-stable) location. The in situ soil water measurement method was selected because the representative location can be easily determined with prior SWC datasets. By measuring SWC only at the most time-stable location (*s*) and future time *t* (S_{ts}), $S_{t\hat{n}}$ can be estimated using (Grayson and Western, 1998):

$$S_{t\hat{n}} = \frac{S_{ts}}{1+\delta_{\hat{ts}}} \quad , \qquad (2)$$

where the *s* was identified using the time stability index of mean absolute bias error (Hu et al., 2010, 2012). The $\delta_{\hat{ts}}$ is the temporal mean relative difference of SWC at the *s*, which was calculated with prior measurements.

Spatial anomaly (Z_{tn}) can be reconstructed by the sum of the product of time-invariant spatial structures (EOFs) and temporally varying coefficients (ECs) using the EOF method (Perry and Niemann, 2007; Joshi and Mohanty, 2010; Vanderlinden et al., 2012). The ECs correspond to the eigenvectors of the matrix of spatial covariance of the Z_{tn}, and the EOFs are obtained by projecting the Z_{tn} onto the matrix ECs as: $\mathrm{EOFs} = Z_{tn}\,\mathrm{EC}s$. The number of EOF (or EC) series equals the number of sampling dates. Each EOF series corresponds to one value at each location, and each EC series has one value at each measurement time. Each EOF is chosen to be orthogonal to other EOFs, and the lower-order EOFs account for as much variance as possible. The sum of variances of all EOFs equals the sum of variances of Z_{tn} from all measurement times.

Usually, a substantial amount of variance can be explained by a small number of EOFs. Johnson and Wichern (2002) suggested the eigenvalue confidence limits method for selecting the number of EOFs. Once the number of significant EOFs at a

confidence level of 95% is selected, Z_{tn} can be estimated as the sum of the product of significant EOFs and associated ECs as:

$$Z_{tn} = \sum \mathrm{EOF}^{sig} \times (\mathrm{EC}^{sig})^{T}, \quad (3)$$

where EOF^{sig} represents the significant EOFs of the Z_{tn} obtained during model development, EC^{sig} is the associated temporally varying coefficient, and the superscript *T* represents matrix transpose. Following Perry and Niemann (2007), the associated significant EC at time *t* (EC_t), is estimated by the cosine relationship between EC and $S_{t\hat{n}}$ developed using prior measurements:

$$\mathrm{EC}_t = a + b\cos\left(\frac{2\pi}{c}\left(S_{t\hat{n}} - d\right)\right), \quad (4)$$

where *a*, *b*, *c*, and *d* are the fitted parameters using prior measurements and $S_{t\hat{n}}$ is estimated from Eq. (2). By using the continuous function, EC_t can be estimated at any $S_{t\hat{n}}$ values, which allows for the estimation of spatially distributed SWC at any soil water conditions.

2.2.2 The TA model

Mittelbach and Seneviratne (2012) decomposed the S_{tn} into a time-stable pattern (i.e., temporal mean) and a temporal anomaly component (Fig. 1):

$$S_{tn} = M_{\hat{t}n} + A_{tn}, \quad (5)$$

where $M_{\hat{t}n}$ is the time-stable pattern (spatial forcing) controlled by "static" factors such as soil properties and topography; A_{tn} refers to the temporal anomaly (lumped temporal forcing and interactions). The variance of SWC ($\sigma^2_{\hat{n}}(S_{tn})$) is the sum of variance of the $M_{\hat{t}n}$ ($\sigma^2_{\hat{n}}(M_{\hat{t}n})$), variance of the A_{tn} ($\sigma^2_{\hat{n}}(A_{tn})$), and two times of covariance between $M_{\hat{t}n}$ and A_{tn} ($2\mathrm{cov}(M_{\hat{t}n}, A_{tn})$), which can be expressed as:

$$\sigma_{\hat{n}}^2\left(S_{tn}\right)=\sigma_{\hat{n}}^2\left(M_{\hat{t}n}\right)+2\mathrm{cov}(M_{\hat{t}n},A_{tn})+\sigma_{\hat{n}}^2\left(A_{tn}\right). \quad (6)$$

Because the A_{tn} in Mittelbach and Seneviratne (2012) is a lumped term, it can be further decomposed into space-invariant temporal anomaly ($A_{t\hat{n}}$, i.e., temporal forcing) and space-variant temporal anomaly (R_{tn} , i.e., interactions) (Vanderlinden et al., 2012). At a watershed scale, the $A_{t\hat{n}}$ is controlled by temporally varying factors such as meteorological variables and vegetation. Positive and negative $A_{t\hat{n}}$ correspond to relatively wet and dry periods, respectively. The R_{tn} refers to the redistribution of $A_{t\hat{n}}$ among different locations due to the interactions between spatial forcing and temporal forcing. For example, soil and topography regulate how much rainfall enters soil and how much water runs off or runs on at a location. This, in turn, dictates vegetation growth in a water-limited environment. Therefore, S_{tn} can also be expressed as (Fig. 1):

$$S_{tn}=M_{\hat{t}n}+A_{t\hat{n}}+R_{tn}. \quad (7)$$

The temporal trends of $A_{t\hat{n}}$ in Eq. (7) and $S_{t\hat{n}}$ in Eq. (1) are the same as both represent temporal forcing. Because the $A_{t\hat{n}}$ is space-invariant and orthogonal to the $M_{\hat{t}n}$ and R_{tn} in a space, $\sigma_{\hat{n}}^2\left(S_{tn}\right)$ in Eq. (6) can also be written as:

$$\sigma_{\hat{n}}^2\left(S_{tn}\right)=\sigma_{\hat{n}}^2\left(M_{\hat{t}n}\right)+2\mathrm{cov}(M_{\hat{t}n},R_{tn})+\sigma_{\hat{n}}^2\left(R_{tn}\right), \quad (8)$$

where $\mathrm{cov}(M_{\hat{t}n},R_{tn})$ is the covariance between the $M_{\hat{t}n}$ and R_{tn}, and $\sigma_{\hat{n}}^2\left(R_{tn}\right)$ is the variance of the R_{tn}. Apparently, $2\mathrm{cov}(M_{\hat{t}n},R_{tn})$ equals $2\mathrm{cov}(M_{\hat{t}n},A_{tn})$, and $\sigma_{\hat{n}}^2\left(R_{tn}\right)$ equals $\sigma_{\hat{n}}^2\left(A_{tn}\right)$. The percent (%) of $\sigma_{\hat{n}}^2\left(M_{\hat{t}n}\right)$, $2\mathrm{cov}(M_{\hat{t}n},R_{tn})$, and $\sigma_{\hat{n}}^2\left(R_{tn}\right)$ out of the $\sigma_{\hat{n}}^2\left(S_{tn}\right)$ are calculated. The $\mathrm{cov}(M_{\hat{t}n},R_{tn})$ can be negative at some conditions, for example, when the depressions correspond to greater $M_{\hat{t}n}$ and

more negative R_{tn} values in the discharge periods. This resulted in percentage of $\sigma^2_{\hat{n}}(M_{\hat{t}n})$ and $\sigma^2_{\hat{n}}(R_{tn})$ > 100% and percentage of $2\mathrm{cov}(M_{\hat{t}n}, R_{tn})$ < 0% (Mittelbach and Seneviratne, 2012; Brocca et al., 2014; Rötzer et al., 2015). If R_{tn} is zero at any time or location, there are no interactions between spatial forcing and temporal forcing, $\sigma^2_{\hat{n}}(S_{tn})$ and the spatial trends of SWC are consistent over time. Therefore, R_{tn} is directly responsible for temporal change in the spatial variability of SWC.

If some underlying spatial patterns exist in R_{tn}, R_{tn} can be reconstructed by the sum of the product of time-invariant spatial structures (EOFs) and time-dependent coefficients (ECs) using the EOF method. Note that the number of EOF (or EC) series also equals the number of sampling dates.

For estimation of spatially distributed SWC, R_{tn} is estimated by the same method as Z_{tn} using Eq. (3). The $M_{\hat{t}n}$ is estimated with prior measurements by:

$$M_{\hat{t}n} = \frac{1}{m}\sum_{j=1}^{m} S_{tn}, \qquad (9)$$

where m is the number of previous measurement times, and $A_{t\hat{n}}$ is estimated by:

$$A_{t\hat{n}} = S_{t\hat{n}} - M_{\hat{t}\hat{n}}, \qquad (10)$$

where $M_{\hat{t}\hat{n}}$ is the spatial mean of $M_{\hat{t}n}$, and $S_{t\hat{n}}$ is estimated from SWC measurements at the most time-stable location using Eq. (2).

The Pearson correlation coefficient (*R*) is used to explore the linear relationships between various spatial components in the two models (i.e., EOF1 of the Z_{tn} in the SA model, $M_{\hat{t}n}$, and EOF1 of the R_{tn} in the TA model) and environmental factors (i.e., soil, vegetative, and topographical properties). The multiple stepwise regressions

285 are conducted to determine the percentage of variations in the spatial components
286 which the controlling factors explain.

287 **2.3 Validation and performance parameter**

288 The TA model is more complicated than the SA model. In order to evaluate the two
289 models for parsimony, AICc values are calculated (Burnham and Anderson, 2002) as:

290 $$\mathrm{AICc} = 2k + n\ln(RSS/n) + 2k(k+1)/(n-k-1), \qquad (11)$$

291 where k is the number of parameters, n is the sample size, and RSS is the residual sum
292 of squares.

293 Both cross validation and split sample validation are used to estimate SWC
294 distribution with both models. For the cross validation, an iterative removal of 1 of the
295 23 dates is made for model development, and the SWC along the transect
296 corresponding to the removed date is estimated iteratively. For the split sample
297 validation, SWC from 14 dates of the first two years (from July 17, 2007 to May 27,
298 2009) is used for model development, and the SWC distribution of 9 dates in the
299 second two years (from July 21, 2009 to September 29, 2011) is estimated.

300 The Nash-Sutcliffe coefficient of efficiency (NSCE) is used to evaluate the quality
301 of estimation of spatially distributed SWC, which is expressed as:

302 $$\mathrm{NSCE} = 1 - \frac{\sigma_{\varepsilon}^2}{\sigma_{measure}^2}, \qquad (12)$$

303 where $\sigma_{measure}^2$ is the variance of measured SWC, and σ_{ε}^2 is the mean squared
304 estimation error. A larger NSCE value implies a better quality of estimation. A paired
305 samples T-test is used to test whether the NSCE values between the TA model and the
306 SA model are statistically significant at $P<0.05$.

Many factors may affect the relative performance of spatially distributed SWC estimation between the TA model and the SA model. First, the degree of outperformance of the TA model over the SA model may depend on the amount of R_{tn} variance considered in the TA model. On one hand, the two models are identical if variance of R_{tn} is close to zero or there are negligible interactions between the spatial and temporal components (Fig. 1). On the other hand, if no underlying spatial patterns exist in the R_{tn} or the underlying spatial patterns accounted for little variance of the R_{tn}, the outperformance will also be very limited. Therefore, the greater the variance of R_{tn} considered in the TA model, the more likely the TA model can outperform the SA model. Second, the way of EOF decomposition may also affect the relative performance. In the SA model, EOF decomposition is performed on lumped time-stable patterns ($M_{\hat{t}n}$) and space-variant temporal anomaly (R_{tn}). In the TA model, however, EOF decomposition is made only on the R_{tn}. In theory, the two models will be identical if the $M_{\hat{t}n}$ and the first underlying spatial pattern (i.e., EOF1) of the R_{tn} were perfectly correlated. If a nonlinear relationship exists between them, lumping the $M_{\hat{t}n}$ and R_{tn} together, as in the SA model, would weaken the model performance as compared to the TA model. From this aspect, the greater deviation from a linear relationship between the $M_{\hat{t}n}$ and EOF1 of the R_{tn}, may lead to a greater outperformance of the TA model over the SA model. Finally, the performances of both models rely on the estimation accuracy of the EC_t which depends on both goodness of fit of the cosine function (i.e., Eq. 4) and estimation accuracy of the $S_{t\hat{n}}$. Because the same $S_{t\hat{n}}$ values are used for the two

models, the relative performance of the two models is related to the goodness of fit of Eq. (4).

3. Results

3.1 Components of SWC and their controls

3.1.1 Spatial mean ($S_{t\hat{n}}$) and spatial anomaly (Z_{tn})

The values of spatial mean ($S_{t\hat{n}}$) in the SA model varied with the seasons (Fig. 3a). In the spring, such as May 2, 2008 and April 20, 2009, snowmelt infiltration resulted in relatively great $S_{t\hat{n}}$ values. In the summer, however, even one month after large rainfall events (such as on July 19, 2008 and June 21, 2009), the high evapotranspiration by fast-growing vegetation resulted in small $S_{t\hat{n}}$ values. The values of $S_{t\hat{n}}$ also varied between inter-annual meteorological conditions. In 2008, there was less precipitation and higher air temperature than in 2010 (Fig. 2). As a result, $S_{t\hat{n}}$ was relatively smaller in 2008 than in 2010.

The spatial patterns of spatial anomaly (Z_{tn}) were similar to those of the original SWC patterns (Fig. 3a). The values of Z_{tn} in wet periods (e.g., May 13, 2011) were much greater than in dry periods (e.g., August 23, 2008) in depressions (e.g., at a distance of 123 and 250 m); at other locations, however, the spatial anomaly was slightly less in wet periods than in dry periods for both soil layers. Moreover, the spatial anomaly in depressions during the wet periods was much greater in the near surface than in the root zone.

When SWCs of all 23 dates were used for model development, only EOF1 was

350 statistically significant (Fig. 4a), which accounted for 84.3% (0–0.2 m) and 86.5%
351 (0–1.0 m) of the variances in the Z_{tn}. Correlation analysis indicated that the spatial
352 pattern of EOF1 in the Z_{tn} was identical to the time-stable patterns ($M_{\hat{t}n}$) in the TA
353 model (R=1.0). The controls of EOF1 was therefore the same as those of $M_{\hat{t}n}$, and
354 will be discussed later. The relationship between associated EC1 and $S_{t\hat{n}}$ can be
355 fitted well by the cosine function (R^2=0.73 at both the near surface and root zone) (Fig.
356 4b).

357 **3.1.2 Time-stable pattern ($M_{\hat{t}n}$), space-invariant temporal anomaly ($A_{t\hat{n}}$), and**
358 **space-variant temporal anomaly (R_{tn})**

359 Figure 3b displays the three components in the TA model. The first component
360 $M_{\hat{t}n}$ fluctuated along the transect, with high values in depressions and low values on
361 knolls; the $M_{\hat{t}n}$ also had greater spatial variability in the near surface (variance
362 =36.7%^{2}) than in the root zone (variance=19.5%^{2}). For both soil layers, SOC, depth to
363 the $CaCO_3$ layer, sand content, and wetness index are the dominant factors of $M_{\hat{t}n}$;
364 they together explained 74.5% (near surface) and 75.6% (root zone) of the variances
365 in the $M_{\hat{t}n}$ (Table 1). In addition, the temporal trend of $A_{t\hat{n}}$ was the same as that of
366 $S_{t\hat{n}}$ in the SA model (Fig. 3a) as both represent temporal forcing.

367 The R_{tn} varied among landscape positions (Fig. 3b). At a sampling distance of
368 123 m (in a depression), R_{tn} was negative in dry periods such as August 23, 2008 and
369 positive in wet periods such as May 13, 2011. This was true for all depressions for
370 both the near surface and the root zone. Therefore, topographically lower positions
371 usually corresponded to more positive R_{tn} during the wet periods and more negative

372 R_{tn} during the dry periods. Furthermore, the absolute values of R_{tn} were generally
373 greater in the near surface than the root zone, indicating a greater space-variant
374 temporal anomaly for shallower depths.

375 The SWC variances and associated components (Eq. 8) also varied with time (Fig.
376 5). Often, wetter conditions corresponded to greater $\sigma^2_{\hat{n}}(S_{tn})$, as further indicated by
377 moderate correlation between $\sigma^2_{\hat{n}}(S_{tn})$ and $S_{t\hat{n}}$ (R^2 of 0.51 and 0.38 for the near
378 surface and the root zone, respectively). This was in agreement with others
379 (Gómez-Plaza et al., 2001; Martínez-Fernández and Ceballos, 2003; Hu et al., 2011).
380 Furthermore, there were greater $\sigma^2_{\hat{n}}(S_{tn})$ values at near surface than in the root zone,
381 indicating greater variability of SWC in the near surface.

382 The time-invariant $\sigma^2_{\hat{n}}(M_{\hat{t}n})$ accounted for the $\sigma^2_{\hat{n}}(S_{tn})$ with percentages
383 ranging from 25 to 795% for the near surface and from 40 to 174% for the root zone
384 (Fig. 5). The $\sigma^2_{\hat{n}}(M_{\hat{t}n})$ exceeded the $\sigma^2_{\hat{n}}(S_{tn})$ mainly under dry conditions, such as
385 July–October in 2008 and 2009. This excess was offset by the $\sigma^2_{\hat{n}}(R_{tn})$ and
386 $2\mathrm{cov}(M_{\hat{t}n}, R_{tn})$, with the latter accounting for the $\sigma^2_{\hat{n}}(S_{tn})$ negatively with mean
387 absolute percentages of 210% for the near surface and 17% for the root zone. In the
388 dry period, the absolute percentage of $2\mathrm{cov}(M_{\hat{t}n}, R_{tn})$ was up to 1327% for the near
389 surface and 122% for the root zone. These values are comparable to those in
390 Mittelbach and Seneviratne (2012) and Brocca et al. (2014).

391 The $\sigma^2_{\hat{n}}(R_{tn})$ accounted for less percentage of the $\sigma^2_{\hat{n}}(S_{tn})$ than other
392 components did (Fig. 5). The percentages of $\sigma^2_{\hat{n}}(R_{tn})$ ranged from 11 to 632%
393 (arithmetic average of 118%) for the near surface and from 6 to 48% (arithmetic

394 average of 19%) for the root zone; the percentage of $\sigma_{\hat{n}}^2(R_{tn})$ tended to be greater in
395 drier periods. This indicates that the space-variant temporal anomaly cannot be
396 ignored, particularly in dry conditions. Furthermore, the percentage of $\sigma_{\hat{n}}^2(R_{tn})$ was
397 greater in the near surface than in the root zone, confirming stronger temporal
398 dynamics of soil water at the near surface. Compared with larger scale studies
399 (Mittelbach and Seneviratne, 2012; Brocca et al., 2014), the percentage of $\sigma_{\hat{n}}^2(R_{tn})$
400 out of the $\sigma_{\hat{n}}^2(S_{tn})$ at the near surface was greater, with a mean percentage of 118%,
401 versus 9–68% in the other, larger scale studies. This indicates that interactions
402 between spatial and temporal forcing were stronger, resulting in relatively more
403 intensive temporal dynamics of soil water in our study area than at larger scales.

404 Three significant EOFs of R_{tn} for both soil layers were identified when SWC of
405 all 23 dates were used for model development. The first three EOFs explained 61.1,
406 13.4, and 8.1% respectively, of the total R_{tn} variance for the near surface, and 44.3,
407 20.2, and 12.4%, respectively, of the total R_{tn} variance in the root zone. Therefore,
408 our hypothesis that underlying spatial patterns exist in the R_{tn} was supported. Due
409 to the negligible contribution of EOF2 and EOF3 to the estimation of spatially
410 distributed SWC, only EOF1 is shown in Fig. 6a. The associated EC1 changed with
411 soil water conditions ($S_{t\hat{n}}$) (Fig. 6b). When SWC was close to average levels, the EC1
412 was close to 0, resulting in negligible R_{tn}. This was in accordance with Mittelbach
413 and Seneviratne (2012) and Brocca et al. (2014), who showed that the spatial variance
414 of the temporal anomaly was the smallest when water contents were close to average
415 levels. The cosine function (Eq. 4) explained a large amount of the variances in EC1

for both soil layers (R^2=0.76 at the near surface and 0.88 in the root zone).

The contribution of EOF1 to the space-variant temporal anomaly can be examined through the product of the EOF1 and the associated EC1. The EC1 values tended to be positive during wet periods and negative during dry periods (Fig. 6b); more positive EOF1 values were usually observed at locations with greater $M_{\hat{t}n}$ values (Figs. 3b and 6a). Therefore, the product of EOF1 and EC1 led to greater temporal SWC dynamics at wetter locations of both layers in both the wet and dry periods.

Depth to the $CaCO_3$ layer and SOC had significant, positive correlations with EOF1 for both soil layers (R ranging from 0.76 to 0.88; Table 1). They jointly accounted for 81.6% (near surface) and 81.0% (root zone) of the variances in EOF1. This implies that locations with a greater depth to the $CaCO_3$ layer and SOC, which correspond to wetter locations such as depressions, usually have greater temporal SWC dynamics during both wet and dry periods.

3.2 Estimation of spatially distributed SWC

When all 23 datasets were used and only EOF1 was considered, the TA model had an AICc value of 4093 for the near surface and 562 for the root zone, while the corresponding values for the SA model were 6370 and 3460. This indicated that even when penalty to complexity was given, the TA model was better than the SA model. The two models in terms of spatially distributed SWC estimation are compared below.

3.2.1 The TA model

The R_{tn} terms and associated EOFs differed slightly with each validation. The number of significant EOFs varied between one (accounting for 60% of the total cases)

438 and three for both soil layers. A paired samples T-test indicated that more EOFs did
439 not result in a significant increase of NSCE in the estimation of spatially distributed
440 SWC for both validation methods. This is also supported by the increasing AICc
441 values with the increasing number of parameters resulting from more EOFs (data not
442 shown). This indicates that higher-order EOFs, even if they are statistically significant,
443 are negligible for SWC prediction. Therefore, SWC distribution was estimated with
444 EOF1 only.

445 Estimated SWCs generally approximated those measured at different soil water
446 conditions during the cross validation (Fig. 7). However, on October 27, 2009, there
447 were unsatisfactory overestimates at the 100–140 and 220–225 m locations near the
448 surface (Fig. 7a). Unsatisfactory NSCE values of -4.05, -1.83, and -3.81 were
449 obtained in the near surface in only three of the 23 dates, which were all in the fall
450 (October 22, 2008, August 27, 2009, and October 27, 2009, respectively). The poor
451 performance obtained with the TA model on those dates (Fig. 8a) was a result of
452 overestimation in depressions, which is shown for example on October 27, 2009 (Fig.
453 7a). These dates also corresponded to a high percentage of $\sigma_{\hat{n}}^2(R_{tn})$ to the $\sigma_{\hat{n}}^2(S_{tn})$
454 (203–439%). For August 23 and September 17 in 2008, which were in dry periods,
455 the percentage of $\sigma_{\hat{n}}^2(R_{tn})$ at the near surface was also high (580 and 630%).
456 Because a fair amount of $\sigma_{\hat{n}}^2(R_{tn})$ was accounted for with the TA model, the TA
457 model performed satisfactorily (NSCE of 0.43 and 0.60). For the remaining 20 dates,
458 the resulting NSCE value ranged from 0.38 to 0.90 in the near surface and from 0.65
459 to 0.96 in the root zone (Fig. 8). This suggests that the TA model was generally

460 satisfactory, with better performance in the root zone than in the near surface.

461 During the split sample validation, the TA model resulted in SWC estimations with
462 NSCE values ranging from 0.61 to 0.85 near the surface and from 0.32 to 0.92 in the
463 root zone, with exception of two days (August 27, 2009 and October 27, 2009 with
464 NSCE values of -2.63 and -5.12, respectively) at 0–0.2 m (Fig. 8). This suggested that
465 the TA model performed well in estimating spatially distributed SWC patterns except
466 on August 27, 2009 and October 27, 2009 at 0–0.2 m. The estimation in the root zone
467 was also generally better than in the near surface.

468 **3.2.2 Comparison with the SA model**

469 One significant EOF of Z_{tn} was identified for both soil layers, irrespective of the
470 validation method. The SA model with only EOF1 produced reasonable SWC
471 estimations for both validations in all dates in the root zone and in every date except
472 five dates (August 23, 2008, September 17, 2008, October 22, 2008, August 27, 2009,
473 and October 27, 2009) in the near surface (Fig. 8). Similarly, when more EOFs were
474 included, NSCE values did not increase significantly (data not shown) and
475 consequently, estimation of spatially distributed SWC was not improved. This was
476 because EOF2 and EOF3 together explained a very limited (<10%) amount of
477 variability of Z_{tn} and thus had low predictive power in terms of variance.

478 The difference in NSCE values between the TA and SA models for both validations
479 are presented in Fig. 9. Generally, the difference decreased as $A_{t\hat{n}}$ increased, and
480 then slightly increased with a further increase in $A_{t\hat{n}}$. A paired samples T-test
481 indicated that the NSCE values of the TA model were significantly (P<0.05) greater

than those of the SA model for both soil layers, irrespective of validation methods. This indicates that the TA model outperformed the SA model, particularly in dry conditions. This was because when the soil was dry, there was a high percentage of $\sigma_{\hat{n}}^2(R_{tn})$, and thus strong variability in the space-variant temporal anomaly.

3.3 Further application at other two sites with different scales

3.3.1 A hillslope in the Chinese Loess Plateau

On average, the $\sigma_{\hat{n}}^2(M_{\hat{t}n})$, $\sigma_{\hat{n}}^2(R_{tn})$, and $2\mathrm{cov}(M_{\hat{t}n}, R_{tn})$ accounted for 53, 74 and -27% out of the $\sigma_{\hat{n}}^2(S_{tn})$, indicating that both time-stable pattern and temporal anomalies were the main contributors to the $\sigma_{\hat{n}}^2(S_{tn})$. The EOF analysis showed that only the EOF1 was statistically significant for both the R_{tn} and Z_{tn}, and the EOF1 explained 23% and 47% of the total variances of R_{tn} and Z_{tn}, respectively. This illustrated that underlying spatial patterns exist in the R_{tn} on the hillslope. Cross validation was used to estimate the spatially distributed SWC along the hillslope. The results showed that the NSCE varied from -4.25 to 0.83 (TA model) and from -4.30 to 0.81 (SA model), with a mean value of 0.25 and 0.19, respectively (Fig. 10a). A paired samples T-test showed that the NSCE values for the TA model were significantly (P<0.05) greater than those for the SA model, indicating that the TA model outperformed the SA model. As Fig. 10a shows, the outperformance was greater when SWC deviated from intermediate conditions, especially for dry conditions, which was similar to the Canadian site.

3.3.2 The GENCAI network in Italy

The $\sigma_{\hat{n}}^2(M_{\hat{t}n})$, $\sigma_{\hat{n}}^2(R_{tn})$, and $2\mathrm{cov}(M_{\hat{t}n}, R_{tn})$ accounted for 38, 68, and -7% out

of the $\sigma_{\hat{n}}^2(S_{tn})$ (Brocca et al., 2014), indicating the dominant role of temporal anomalies in SWC variability. The first three EOFs of the R_{tn} explained 19, 16, and 8% of the total $\sigma_{\hat{n}}^2(R_{tn})$, and no EOFs were statistically significant, indicating that no underlying spatial patterns exist in the R_{tn}. The EOF1 of the Z_{tn} was significant and accounted for 37% of the variances in the Z_{tn}. Although the EOF1 of the R_{tn} was not significant, it was considered in the TA model for estimating spatially distributed SWC. The cross validation indicates that the NSCE varied from -0.79 to 0.50 (TA model) and from -0.87 to 0.56 (SA model), with mean values of 0.09 and 0.08, respectively (Fig. 10b). The SWC estimation based on these two models was not satisfactory except for a few days. As Fig. 10b shows, the differences in NSCE values between the two models were scattered around 0. A paired samples T-test showed that the NSCE values between the TA model and the SA model were not significant (P<0.05), indicating no differences in estimating spatially distributed SWC between these two models.

4 Discussion

4.1 Controls of the $M_{\hat{tn}}$ and R_{tn}

The R_{tn} played an important role in the temporal change in spatial patterns of the SWC. The underlying spatial patterns and physical meaning in the R_{tn} were examined in our study for the first time. Although three significant EOFs of the R_{tn} existed in some cases, only EOF1 rather than higher-order EOFs of the R_{tn} should be considered for the spatially distributed SWC estimation. Among many factors

influencing the EOF1 of the R_{tn}, depth to the $CaCO_3$ layer followed by the SOC, were the most important factors. Depressions have deeper $CaCO_3$ layers than knolls, and the shallow $CaCO_3$ layer on knolls limited water infiltration during rainfall or snowmelt, resulting in less water recharge on knolls than in depressions. The depth to $CaCO_3$ layer and SOC were negatively correlated with elevation (R=-0.54, P<0.01). Therefore, the influence of depth to $CaCO_3$ layer and SOC partially reflected the role of topography in driving snowmelt runoff along slopes in the spring, which contributes to increasing water recharge in depressions. As already demonstrated, topographically lower positions corresponded to more negative R_{tn} during the dry periods. This implies that depressions lost more water during discharge. This is because depressions usually corresponded to vegetation with a larger leaf area index, which would result in higher evapotranspiration and more water loss during discharge periods.

As Table 1 shows, both the depth to the $CaCO_3$ layer and SOC controlled the $M_{\hat{t}n}$. This was because deeper $CaCO_3$ layers and higher SOC were observed in depressions where soils were usually wetter in most of the year because of the snowmelt runoff in the spring and rainfall runoff in the summer and autumn (van der Kamp et al., 2003). Therefore, the roles of soil and topography were two-fold: On one hand, they were highly correlated with the time-stable patterns and thus the time stability of SWC (Gómez-Plaza et al., 2000; Mohanty and Skaggs, 2001; Grant et al., 2004); On the other hand, soil and topography, interplaying with temporal forcing, triggered local-specific soil water change and destroyed time stability of SWC. Their roles in

protecting time stability persisted, but their roles in destroying time stability varied with time. Greater $\sigma_{\hat{n}}^2(R_{tn})$ implies greater contribution of these factors in soil water dynamics, resulting in less time stability of SWC.

4.2 Model performance for spatially distributed SWC estimation

The outperformance of the TA model for estimating spatial SWC at the Canadian site and Chinese site can be partly explained by the high percentages (average of 19–118%) of the $\sigma_{\hat{n}}^2(R_{tn})$ out of the total variance. When SWC is close to average levels, R_{tn} is also close to zero, resulting in negligible percentage of $\sigma_{\hat{n}}^2(R_{tn})$. In this case, the soil water patterns are stable in time, the SA model performs well, and there will be little differences between these two models. As is well known, the spatial patterns in soil water content are inherently time unstable. For example, when evapotranspiration becomes the dominant process at the small watershed scale, more water will be lost in depressions due to the denser vegetation than on knolls (Millar, 1971; Biswas et al., 2012), effectively diminishing the spatial patterns and increasing temporal instability. In this case, the $\sigma_{\hat{n}}^2(R_{tn})$ accounts for more percentage of the total variance (e.g., high up to 632%) and the TA model may outperform the SA model. This explained why the outperformance of the TA model was more obvious in the dry conditions. For the GENCAI network in Italy, although the $\sigma_{\hat{n}}^2(R_{tn})$ accounted for 68% of the total variance, the performance of the TA model was identical to the SA model. This was because there were no underlying spatial patterns in the R_{tn}. Similarly, because the first underlying spatial pattern (i.e., EOF1) explained greater percentages of the $\sigma_{\hat{n}}^2(R_{tn})$ at the Canadian site (44–61%) than the

569 Chinese site (23%), the outperformance of the TA model over the SA model was more
570 obvious at the former site (Fig. 9 and 10a). Therefore, the TA model is advantageous
571 only if the percentage of $\sigma_{\hat{n}}^2(R_{tn})$ out of the total variance is substantial and
572 underlying spatial patterns exist in the R_{tn}.

573 The existence of underlying spatial patterns in the R_{tn} is related to the controlling
574 factors, which may be scale-specific. At small scales, "static" factors such as the depth
575 to the $CaCO_3$ layer and SOC at the Canadian site may affect not only the time-stable
576 patterns but also the R_{tn}. The persistent influence of "static" factors on the R_{tn}
577 resulted in significant underlying spatial patterns in the R_{tn}. Thus, the TA model
578 outperformed the SA model at the small scales. At large scales such as the basin scale
579 or greater, time-stable patterns may be controlled by, in addition to soil and
580 topography (Mittelbach and Seneviratne, 2012), the climate gradient (Sherratt and
581 Wheater, 1984); at those scales, R_{tn} is more likely to be controlled by the
582 meteorological anomaly (i.e., spatially random variation) (Walsh and Mostek, 1980),
583 and the effects of soil and topography may be reduced. Consequently, spatial patterns
584 in the R_{tn} may be weakened and the TA model may have no advantages over the SA
585 model such as for the Italian site.

586 The $M_{\hat{tn}}$ and the underlying spatial patterns (EOF1) in the R_{tn} were controlled
587 by the same spatial forcing (e.g., depth to $CaCO_3$ layer and SOC) at the Canadian site
588 (Table 1), and they were correlated with an R^2 of 0.83 for the near surface and 0.42 for
589 the root zone. Although the relationships between $M_{\hat{tn}}$ and R_{tn} were strong, they
590 were not strictly linear, suggesting that $M_{\hat{tn}}$ and R_{tn} were affected differently by

591 these factors. Therefore, the nonlinear relationship between $M_{\hat{t}n}$ and R_{tn} partially
592 contributed to the outperformance of the TA model over the SA model.

593 The relationship between the $S_{t\hat{n}}$ and EC1 was better fitted by the cosine function
594 in the TA model than the SA model (Figs. 4b and 6b), with R^2 of 0.76 versus 0.73 in
595 the near surface and 0.88 versus 0.73 in the root zone. The reduced scatter in the $S_{t\hat{n}}$
596 and EC1 relationship for the TA model may also partly explain the outperformance of
597 the TA model over the SA model.

598 Therefore, the outperformance of the TA model over the SA model depends on
599 counterbalance among the variance of R_{tn} explained in the TA model, the linear
600 correlation between the $M_{\hat{t}n}$ and EOF1 of the R_{tn}, and the goodness of fit for the
601 $S_{t\hat{n}}$ and EC1 relationship. For example, the variance of EOF1 in the R_{tn} for the
602 near surface (i.e., 264%^{2}) was much greater than that for the root zone (i.e., 43%^{2}).
603 However, $M_{\hat{t}n}$ and underlying spatial patterns (EOF1) in the R_{tn} in the root zone
604 deviated more from a linear relationship, and the reduced scatter in the $S_{t\hat{n}}$ and EC1
605 relationship in the TA model was more obviously in the root zone than in the near
606 surface. As a result, the outperformance of the TA model was comparable between the
607 near surface and root zone at the Canadian site (Fig. 9).

608 In the real world, the relations between the $M_{\hat{t}n}$ and underlying spatial patterns in
609 the R_{tn} may rarely be perfectly linear. Therefore, when underlying spatial patterns
610 exist in the R_{tn} and the R_{tn} has substantial variances, the TA model is preferable
611 to the SA model for the estimation of spatially distributed SWC. On the other hand,
612 when underlying spatial patterns do not exist in the R_{tn} or the R_{tn} has negligible

613 variances, the SA model may be selected although these two models yield the same
614 quality of SWC estimation. This is because the TA model needs one more spatial
615 parameter (i.e., $M_{\hat{t}n}$) than the SA model.

616 Previous studies on SWC decomposition mainly focus on near surface layers
617 (Jawson and Niemann, 2007; Perry and Niemann, 2007, 2008; Joshi and Mohanty,
618 2010; Korres et al., 2010; Busch et al., 2012). This study decomposed spatiotemporal
619 SWC using the TA model for both the near surface and the root zone. The results
620 showed that the estimation of spatially distributed SWC at small watershed scales was
621 improved by the TA method that considers the R_{tn}. The $\sigma^2_{\hat{n}}\left(M_{\hat{t}n}\right)$ was greater than
622 the $\sigma^2_{\hat{n}}\left(R_{tn}\right)$ (Fig. 5), indicating that time stability was more important than time
623 instability for SWC estimation. For the three dates in the fall (i.e., October 22, 2008,
624 August 27, 2009, and October 27, 2009), strong evapotranspiration and deep drainage
625 in depressions resulted in a much lower SWC at the near surface than in the spring.
626 This resulted in reduced time stability of SWC patterns and poor performance of both
627 models in terms of SWC evaluation (Fig. 8a). Because of the stronger time stability of
628 SWC in deeper soil layers (Biswas and Si, 2011), SWC evaluation was more accurate
629 for soil layers extending from the surface to greater depth. This is particularly
630 important because SWC data for deeper soil layers in a watershed is more difficult to
631 collect than that of surface soil.

632 # 5 Conclusions

633 The TA model was used to decompose spatiotemporal SWC into time-stable

patterns $M_{\hat{t}n}$, space-invariant temporal anomaly $A_{t\hat{n}}$, and space-variant temporal anomaly R_{tn}. This study indicated that underlying spatial patterns may exist in the R_{tn} at small scales (e.g., small watersheds and hillslope) but may not exist at large scales such as the GENCAI network (~250 km^2) in Italy. This was because the R_{tn} at small scales was driven by "static" factors such as depth to the $CaCO_3$ layer and SOC at the Canadian site, while the R_{tn} at large scales may be dominated by "dynamic" factors such as meteorological anomaly. Compared to the SA model, estimation of spatially distributed SWC was improved with the TA model at small watershed scales. This was because the TA model considered a fair amount of spatial variance in the R_{tn}, which was ignored in the SA model. Furthermore, the improved performance was observed mainly when there was less or more soil water than the average level, especially in drier conditions due to the high $\sigma_{\hat{n}}^2(R_{tn})$ value.

This study showed that outperformance of the TA model over the SA model is possible when $\sigma_{\hat{n}}^2(R_{tn})$ accounts for substantial variance of SWC, and significant spatial patterns (or EOFs) exist in the R_{tn}. Further application of the TA model for the estimation of spatially distributed SWC at different scales and hydrological backgrounds is recommended. If the TA model parameters (i.e., $M_{\hat{t}n}$, EOF1 of the R_{tn}, and relationship between EC and $S_{t\hat{n}}$) are obtained from historical in-situ SWC datasets, a detailed spatially distributed SWC of near surface soil at watershed scales can be constructed from remotely sensed SWC. Note that both models rely on in-situ SWC measurements for model parameters. Therefore, future research should be conducted to estimate spatially distributed SWC in un-gauged watersheds based on

656 the estimation of the model parameters using pedotransfer functions. The codes for
657 decomposing SWC with the SA and TA models and related EOF analysis were written
658 in Matlab and are freely available from the authors upon request.

659 Acknowledgements

660 This project was funded by the National Science Foundation of China (K305021308)
661 and the Natural Sciences and Engineering Research Council (NSERC) of Canada. We
662 thank Dr. Asim Biswas, Dr. Henry Wai Chau, Mr. Trent Pernitsky, and Mr. Eric Neil
663 for their help in data collection. We thank the anonymous reviewers and the Editor for
664 their constructive comments.

665 References

666 Biswas, A., Chau, H. W., Bedard-Haughn, A., and Si, B. C.: Factors controlling soil
667 water storage in the Hummocky landscape of the Prairie Pothole region of North
668 America, Can. J. Soil Sci., 92, 649–663, doi: 10.4141/CJSS2011-045, 2012.
669 Biswas, A. and Si, B. C.: Scales and locations of time stability of soil water storage in
670 a hummocky landscape, J. Hydrol., 408, 100–112, doi: 10.1016/j.jhydrol.2011.07.027,
671 2011.
672 Blöschl, G., Komma, J., and Hasenauer, S.: Hydrological downscaling of soil
673 moisture, Final report to the H-SAF (Hydrology Satellite Application Facility) via the
674 Austrian Central Institute for Meteorology and Geodynamics (ZAMG), Vienna
675 University of Technology, A-1040 Vienna, Austria, 2009.

676 Brocca, L., Melone, F., Moramarco, T., and Morbidelli, R.: Soil moisture temporal
677 stability over experimental areas in Central Italy, Geoderma, 148, 364–374, doi:
678 10.1016/j.geoderma.2008.11.004, 2009.
679 Brocca, L., Tullo, T., Melone, F., Moramarco, T., and Morbidelli, R.: Catchment scale
680 soil moisture spatial-temporal variability, J. Hydrol., 422-423, 63–75,
681 doi:10.1016/j.jhydrol.2011.12.039, 2012.
682 Brocca, L., Zucco, G., Mittelbach, H., Moramarco, T., and Seneviratne, S. I.: Absolute
683 versus temporal anomaly and percent of saturation soil moisture spatial variability for
684 six networks worldwide, Water Resour. Res., 50, 5560–5576, doi:
685 10.1002/2014WR015684, 2014.
686 Brocca, L., Zucco, G., Moramarco, T., and Morbidelli, R.: Developing and testing a
687 long-term soil moisture dataset at the catchment scale, J. Hydrol., 490, 144–151, doi:
688 10.1016/j.jhydrol.2013.03.029, 2013.
689 Burnham, K. P. and Anderson, D. R.: Model selection and multimodel inference: A
690 practical information-theoretic approach (2nd ed.), Springer-Verlag, New York, 2002.
691 Busch, F. A., Niemann, J. D., and Coleman, M.: Evaluation of an empirical
692 orthogonal function-based method to downscale soil moisture patterns based on
693 topographical attributes, Hydrol. Process., 26, 2696–2709, doi: 10.1002/hyp.8363,
694 2012.
695 Champagne, C., Berg, A. A., McNairn, H., Drewitt, G., and Huffman, T.: Evaluation
696 of soil moisture extremes for agricultural productivity in the Canadian prairies, Agric.
697 For. Meteorol., 165, 1–11, doi: 10.1016/j.agrformet.2012.06.003, 2012.

698 Famiglietti, J. S., Rudnicki, J. W., and Rodell, M.: Variability in surface moisture
699 content along a hillslope transect: Rattlesnake Hill, Texas, J. Hydrol., 210, 259–281,
700 doi: 10.1016/S0022-1694(98)00187-5, 1998.
701 Gómez-Plaza, A., Alvarez-Rogel, J., Albaladejo, J., and Castillo, V. M.: Spatial
702 patterns and temporal stability of soil moisture across a range of scales in a semi-arid
703 environment, Hydrol. Process., 14, 1261–1277, doi:
704 10.1002/(SICI)1099-1085(200005)14:7<1261::AID-HYP40>3.0.CO;2-D, 2000.
705 Gómez-Plaza, A., Martínez-Mena, M., Albaladejo, J., and Castillo, V. M.: Factors
706 regulating spatial distribution of soil water content in small semiarid catchments, J.
707 Hydrol., 253, 211–226, doi: 10.1016/S0022-1694(01)00483-8, 2001.
708 Grant, L., Seyfried, M., and McNamara, J.: Spatial variation and temporal stability of
709 soil water in a snow-dominated, mountain catchment, Hydrol. Process., 18,
710 3493–3511, doi: 10.1002/hyp.5789, 2004.
711 Grayson, R. B. and Western, A. W.: Towards areal estimation of soil water content
712 from point measurements: Time and space stability of mean response, J. Hydrol., 207,
713 68–82, doi: 10.1016/S0022-1694(98)00096-1, 1998.
714 Hu, W., Shao, M. A., Han, F. P., and Reichardt, K.: Spatio-temporal variability
715 behavior of land surface soil water content in shrub- and grass-land, Geoderma, 162,
716 260–272, doi: 10.1016/j.geoderma.2011.02.008, 2011.
717 Hu, W., Shao, M. A., and Reichardt, K.: Using a new criterion to identify sites for
718 mean soil water storage evaluation, Soil Sci. Soc. Am. J., 74, 762–773, doi:
719 10.2136/sssaj2009.0235, 2010.

720 Hu, W., Tallon, L. K., and Si, B. C.: Evaluation of time stability indices for soil water
721 storage upscaling, J. Hydrol., 475, 229–241, doi: 10.1016/j.jhydrol.2012.09.050,
722 2012.
723 Jawson, S. D. and Niemann, J. D.: Spatial patterns from EOF analysis of soil moisture
724 at a large scale and their dependence on soil, land-use, and topographic properties,
725 Adv. Water Resour., 30, 366–381, doi:10.1016/j.advwatres.2006.05.006, 2007.
726 Jia, Y. H. and Shao, M. A.: Temporal stability of soil water storage under four types of
727 revegetation on the northern Loess Plateau of China, Agric. Water Manage., 117,
728 33–42, doi: 10.1016/j.agwat.2012.10.013, 2013.
729 Johnson, R. A. and Wichern, D. W.: Applied multivariate statistical analysis, Prentice
730 Hall, Upper Saddle River, New Jersey, 2002.
731 Joshi, C. and Mohanty, B. P.: Physical controls of near-surface soil moisture across
732 varying spatial scales in an agricultural landscape during SMEX02, Water Resour.
733 Res., 46, doi: 10.1029/2010WR009152, 2010.
734 Korres, W., Koyama, C. N., Fiener, P., and Schneider, K.: Analysis of surface soil
735 moisture patterns in agricultural landscapes using Empirical Orthogonal Functions,
736 Hydrol. Earth Syst. Sci., 14, 751–764, doi: 10.5194/hess-14-751-2010, 2010.
737 Mart ínez-Fern ández, J. and Ceballos, A.: Temporal stability of soil moisture in a
738 large-field experiment in Spain, Soil Sci. Soc. Am. J., 67, 1647–1656, 2003.
739 Millar, J. B.: Shoreline-area ratios as a factor in rate of water loss from small sloughs,
740 J. Hydrol., 14, 259–284, doi: 10.1016/0022-1694(71)90038-2, 1971.
741 Mittelbach, H. and Seneviratne, I.: A new perspective on the spatio-temporal

742 variability of soil moisture: Temporal dynamics versus time-invariant contributions,
743 Hydrol. Earth Syst. Sci., 16, 2169–2179, doi: 10.5194/hess-16-2169-2012, 2012.
744 Mohanty, B. P. and Skaggs, T. H.: Spatio-temporal evolution and time–stable
745 characteristics of soil moisture within remote sensing footprints with varying soil
746 slope and vegetation, Adv. Water Resour., 24, 1051–1067, doi:
747 10.1016/S0309-1708(01)00034-3, 2001.
748 Peel, M. C., Finlayson, B. L., and McMahon, T. A.: Updated world map of the
749 Köppen-Geiger climate classification, Hydrol. Earth Syst. Sci., 11, 1633–1644,
750 doi:10.5194/hess-11-1633-2007, 2007.
751 Perry, M. A. and Niemann J. D.: Analysis and estimation of soil moisture at the
752 catchment scale using EOFs, J. Hydrol., 334, 388–404, doi:
753 10.1016/j.jhydrol.2006.10.014, 2007.
754 Perry, M. A. and Niemann J. D.: Generation of soil moisture patterns at the catchment
755 scale by EOF interpolation, Hydrol. Earth Syst. Sci., 12, 39–53,
756 doi:10.5194/hess-12-39-2008, 2008.
757 Robinson, D. A., Campbell, C. S., Hopmans, J. W., Hornbuckle, B. K., Jones, S. B.,
758 Knight, R., Ogden, F., Selker, J., and Wendroth, O.: Soil moisture measurement for
759 ecological and hydrological watershed-scale observatories: A review, Vadose Zone J.,
760 7, 358–389, doi: 10.2136/vzj2007.0143, 2008.
761 Rötzer, K., Montzka, C., and Vereecken, H.: Spatio-temporal variability of global soil
762 moisture products, J. Hydrol., 522, 187–202, doi: 10.1016/j.jhydrol.2014.12.038,
763 2015.

She, D. L., Liu, D. D., Peng, S. Z., and Shao, M. A.: Multiscale influences of soil properties on soil water content distribution in a watershed on the Chinese Loess Plateau, Soil Sci., 178, 530–539, doi: 10.1016/j.jhydrol.2014.08.034, 2013a.

She, D. L., Xia, Y. Q., Shao, M. A., Peng, S. Z., and Yu, S. E.: Transpiration and canopy conductance of Caragana Korshinskii trees in response to soil moisture in sand land of China, Agrofor. Syst., 87, 667–678, doi: 10.1007/s10457-012-9587-4, 2013b.

Sherratt, D. J. and Wheater, H. S.: The use of surface-resistance soil-moisture relationships in soil-water budget models, Agric. For. Meteorol., 31, 143–157, doi: 10.1016/0168-1923(84)90016-9, 1984.

Soil Survey Staff: Soil Taxonomy, 11th edition, USDA National Resources Conservation Services, Washington DC, 2010.

Starr, G. C.: Assessing temporal stability and spatial variability of soil water patterns with implications for precision water management, Agric. Water Manage., 72, 223–243, doi: 10.1016/j.agwat.2004.09.020, 2005.

Vachaud, G., De Silans, A. P., Balabanis, P., and Vauclin, M.: Temporal stability of spatially measured soil water probability density function, Soil Sci. Soc. Am. J., 49, 822–828, 1985.

van der Kamp, G., Hayashi, M., and Gallen, D.: Comparing the hydrology of grassed and cultivated catchments in the semi-arid Canadian prairies, Hydrol. Process., 17, 559–575, doi: 10.1002/hyp.1157, 2003.

Vanderlinden, K., Vereecken, H., Hardelauf, H., Herbst, M., Martinez, G., Cosh, M.

786 H., and Pachepsky, Y. A.: Temporal stability of soil water contents: A review of data
787 and analyses, Vadose Zone J., 11, 4, doi: 10.2136/vzj2011.0178, 2012.
788 Vereecken, H., Kamai, T., Harter, T., Kasteel, R., Hopmans, J., and Vanderborght, J.:
789 Explaining soil moisture variability as a function of mean soil moisture: A stochastic
790 unsaturated flow perspective, Geophys. Res. Lett., 34, L22402, doi:
791 10.1029/2007GL031813, 2007.
792 Venkatesh, B., Nandagiri, L., Purandara, B. K., and Reddy, V. B.: Modelling soil
793 moisture under different land covers in a sub-humid environment of Western Ghats,
794 India, J. Earth Syst. Sci., 120, 387–398, 2011.
795 Walsh, J. E. and Mostek, A.: A quantitative-analysis of meteorological anomaly
796 patterns over the United-States, 1900–1977, Mon. Weather Rev., 108, 615–630, doi:
797 10.1175/1520-0493(1980)108<0615:AQAOMA>2.0.CO;2, 1980.
798 Wang, Y. Q., Shao, M. A., Liu. Z. P., and Warrington, D. N.: Regional spatial pattern
799 of deep soil water content and its influencing factors, Hydrolog. Sci. J., 57, 265–281,
800 doi: 10.1080/02626667.2011.644243, 2012.
801 Ward, P. R., Flower, K. C., Cordingley, N., Weeks, C., and Micin, S. F.: Soil water
802 balance with cover crops and conservation agriculture in a Mediterranean climate,
803 Field Crop. Res., 132, 33–39, doi: 10.1016/j.fcr.2011.10.017, 2012.
804 Zhao, Y., Peth, S., Wang, X. Y., Lin, H., and Horn, R.: Controls of surface soil
805 moisture spatial patterns and their temporal stability in a semi-arid steppe, Hydrol.
806 Process., 24, 2507–2519, doi: 10.1002/hyp.7665, 2010.

807 ## Figure captions

808 **Figure 1.** Decomposition of spatiotemporal soil water content (SWC) in different
809 models.

810 **Figure 2.** Daily mean air temperature and precipitation during the study period.

811 **Figure 3.** Components of soil water content in (a) the SA model (spatial mean soil
812 water content $S_{t\hat{n}}$ and spatial anomaly Z_{tn}) and in (b) the TA model (time-stable
813 pattern $M_{\hat{t}n}$, space-invariant temporal anomaly $A_{t\hat{n}}$, and space-variant temporal
814 anomaly R_{tn}) for 0–0.2 and 0–1.0 m. Also shown is the elevation.

815 **Figure 4.** (a) The EOF1 of the spatial anomaly Z_{tn} and (b) relationships of
816 associated EC1 versus spatial mean soil water content Z_{tn} fitted by the cosine
817 function (Eq. 4).

818 **Figure 5.** Spatial variances of different components in Eq. (8) expressed in $\%^2$ (upper
819 panel) and as percentage (lower panel) for (a) 0–0.2 and (b) 0–1.0 m. Spatial mean
820 soil water content $S_{t\hat{n}}$ on each measurement day is also shown.

821 **Figure 6.** (a) The EOF1 of the space-variant temporal anomaly R_{tn} and (b)
822 relationships of associated EC1 versus spatial mean soil water content $S_{t\hat{n}}$ fitted by
823 the cosine function (Eq. 4).

824 **Figure 7.** Estimated soil water content (SWC) versus measured SWC for three dates
825 at different soil water conditions (August 23, 2008, October 27, 2009, and May 13,
826 2011 are associated with relatively dry, medium, and wet days, respectively) using the
827 TA model for (a) 0–0.2 and (b) 0–1.0 m.

828 **Figure 8.** The Nash-Sutcliffe coefficient of efficiency (NSCE) of soil water content

829 estimation using the TA and SA models for (a) 0–0.2 and (b) 0–1.0 m for both cross
830 validation (CV) and split sample validation (SV). At 0–0.2 m, three dates (October 22,
831 2008, August 27, 2009, and October 27, 2009) as indicated by green lines present
832 negative NSCE values (-4.05, -1.83, and -3.81, respectively, for the CV on the three
833 dates; -2.63 and -5.12, respectively, for the SV on the latter two dates). Spatial mean
834 soil water content $S_{t\hat{n}}$ on each measurement day is also shown.

835 **Figure 9.** Nash-Sutcliffe coefficient of efficiency (NSCE) difference between the TA
836 and SA models in terms of soil water content estimation using both cross validation
837 (CV) and split sample validation (SV) as a function of space-invariant temporal
838 anomaly $A_{t\hat{n}}$ for (a) 0–0.2 and (b) 0–1.0 m.

839 **Figure 10.** Nash-Sutcliffe coefficient of efficiency (NSCE) difference between the TA
840 and SA models in terms of soil water content estimation using cross validation as a
841 function of space-invariant temporal anomaly $A_{t\hat{n}}$ for (a) 0–0.06 m of the Chinese
842 Loess Plateau hillslope and (b) 0–0.15 m of the GENCAI network in Italy. The NSCE
843 values for both models are also shown.

Table 1. Pearson correlation coefficients between time-stable pattern $M_{\hat{t}n}$, EOF1 of space-variant temporal anomaly R_{tn} and various properties.

	0–0.2 m		0–1.0 m	
	$M_{\hat{t}n}$	EOF1	$M_{\hat{t}n}$	EOF1
Sand content	-0.52**	-0.36**	-0.66**	-0.26**
Silt content	0.29**	0.14	0.40**	0.06
Clay content	0.43**	0.38**	0.51**	0.33**
Organic carbon	0.78**	0.83**	0.73**	0.76**
Wetness index	0.64**	0.59**	0.68**	0.56**
Depth to $CaCO_3$ layer	0.77**	0.84**	0.65**	0.88**
A horizon depth	0.51**	0.62**	0.44**	0.65**
C horizon depth	0.66**	0.69**	0.58**	0.76**
Bulk density	-0.58**	-0.67**	-0.46**	-0.62**
Elevation	-0.24**	-0.28**	-0.24**	-0.32**
Specific contributing area	0.20*	0.24**	0.24**	0.23**
Convergence index	-0.58**	-0.56**	-0.55**	-0.58**
Curvature	-0.10	-0.08	-0.19*	-0.16
Cos(aspect)	0.05	0.04	0.08	0.05
Gradient	-0.12	-0.09	-0.21*	-0.02
Slope	-0.51**	-0.48**	-0.56**	-0.44**
Upslope length	0.19*	0.21*	0.21*	0.25**
Solar radiation	-0.07	0.03	-0.11	0.08
Flow connectivity	0.45**	0.43**	0.49**	0.49**
Leaf area index	-0.07	0.06	-0.10	-0.14
Variance explained[1]	74.5%	81.6%	75.6%	81.0%

[1]percent of variance explained by the controlling factors obtained by the multiple stepwise regressions.
*Significant at $P<0.05$; ** Significant at $P<0.01$.

Table A1. Notations.

$M_{\hat{t}\hat{n}}$	spatial mean of $M_{\hat{t}n}$
R_{tn}	space-variant temporal anomaly of SWC at location *n* and time *t*
$A_{t\hat{n}}$	space-invariant temporal anomaly of SWC at time *t*
Z_{tn}	spatial anomaly of SWC at location *n* and time *t*
$S_{t\hat{n}}$	spatial mean SWC at time *t*
$\sigma^2_{\hat{n}}$	spatial variance
A_{tn}	temporal anomaly of SWC at location *n* and time *t*
$\delta_{\hat{t}n}$	temporal mean relative difference of SWC at location *n*
COV	spatial covariance
S_{tn}	SWC at location *n* and time *t*
$M_{\hat{t}n}$	time-stable pattern of SWC
ECs	temporally-varying coefficients of R_{tn} (or Z_{tn})
EOFs	time-invariant spatial structures of R_{tn} (or Z_{tn})
NSCE	Nash-Sutcliffe coefficient of efficiency
R	Pearson correlation coefficient
SWC	soil water content

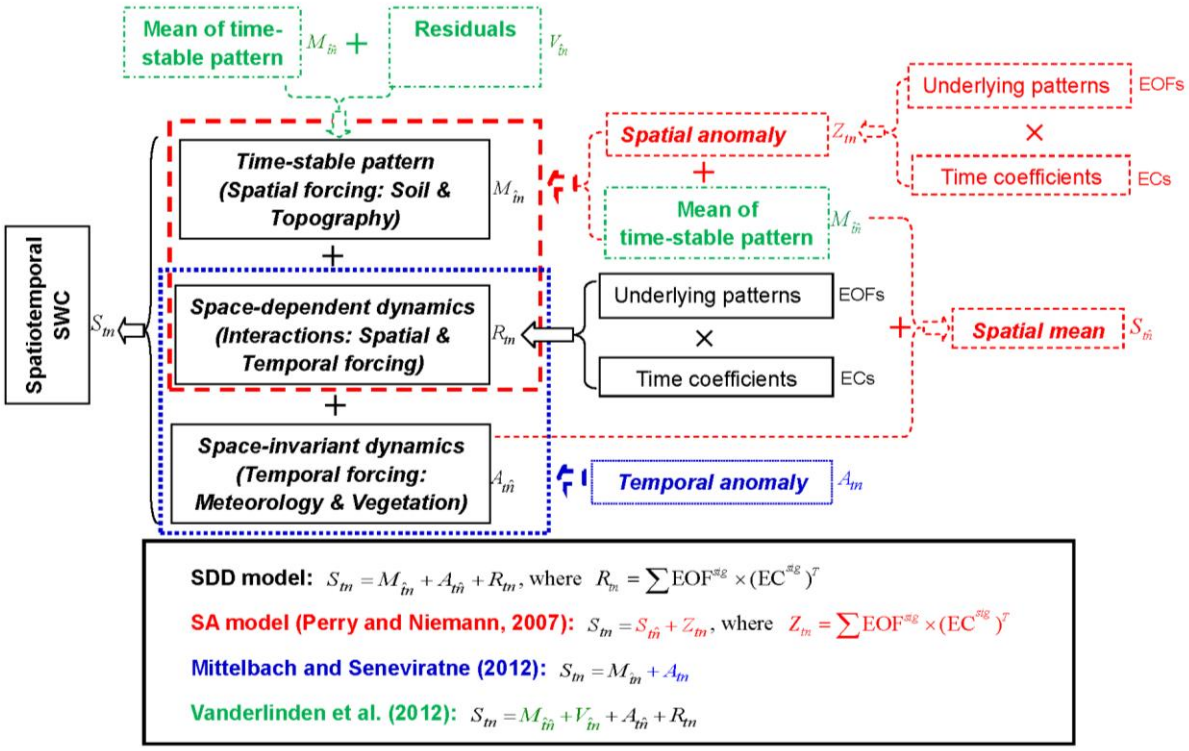

Fig. 1. Decomposition of spatiotemporal soil water content (SWC) in different models.

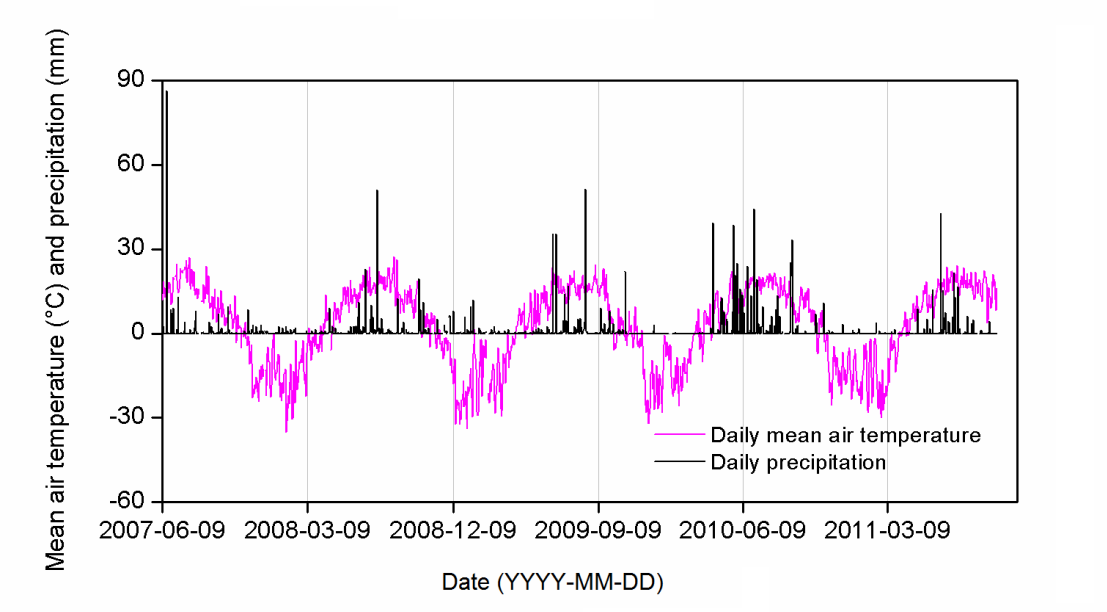

Fig. 2. Daily mean air temperature and precipitation during the study period.

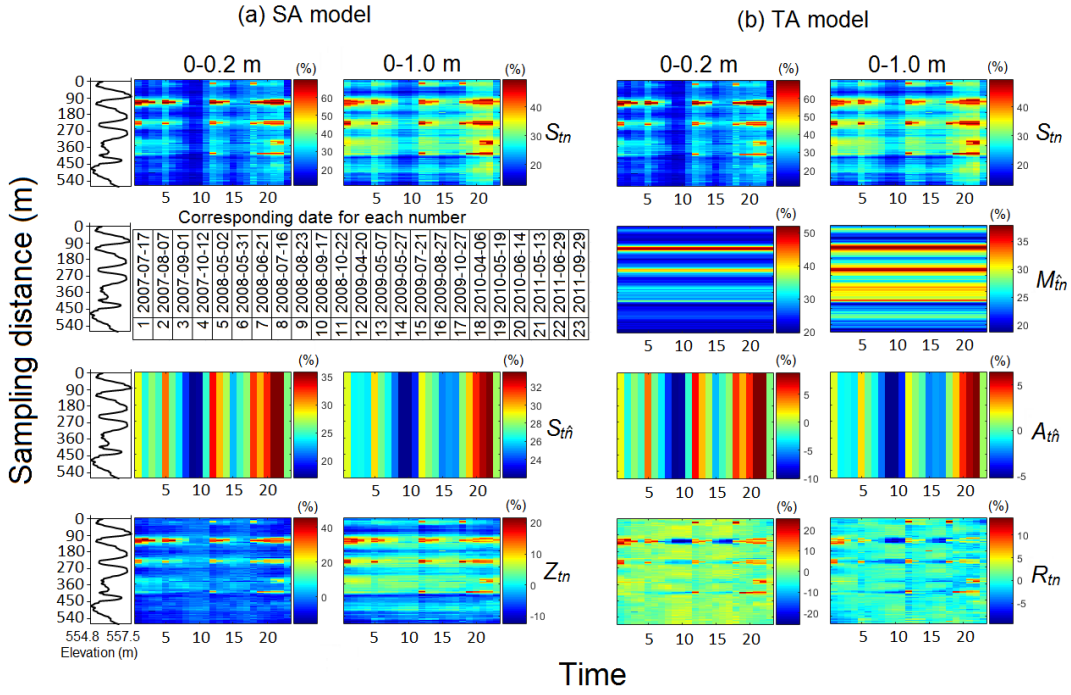

Fig. 3. Components of soil water content in (a) the SA model (spatial mean soil water content $S_{t\hat{n}}$ and spatial anomaly Z_{tn}) and in (b) the TA model (time-stable pattern $M_{\hat{t}n}$, space-invariant temporal anomaly $A_{t\hat{n}}$, and space-variant temporal anomaly R_{tn}) for 0–0.2 and 0–1.0 m. Also shown is the elevation.

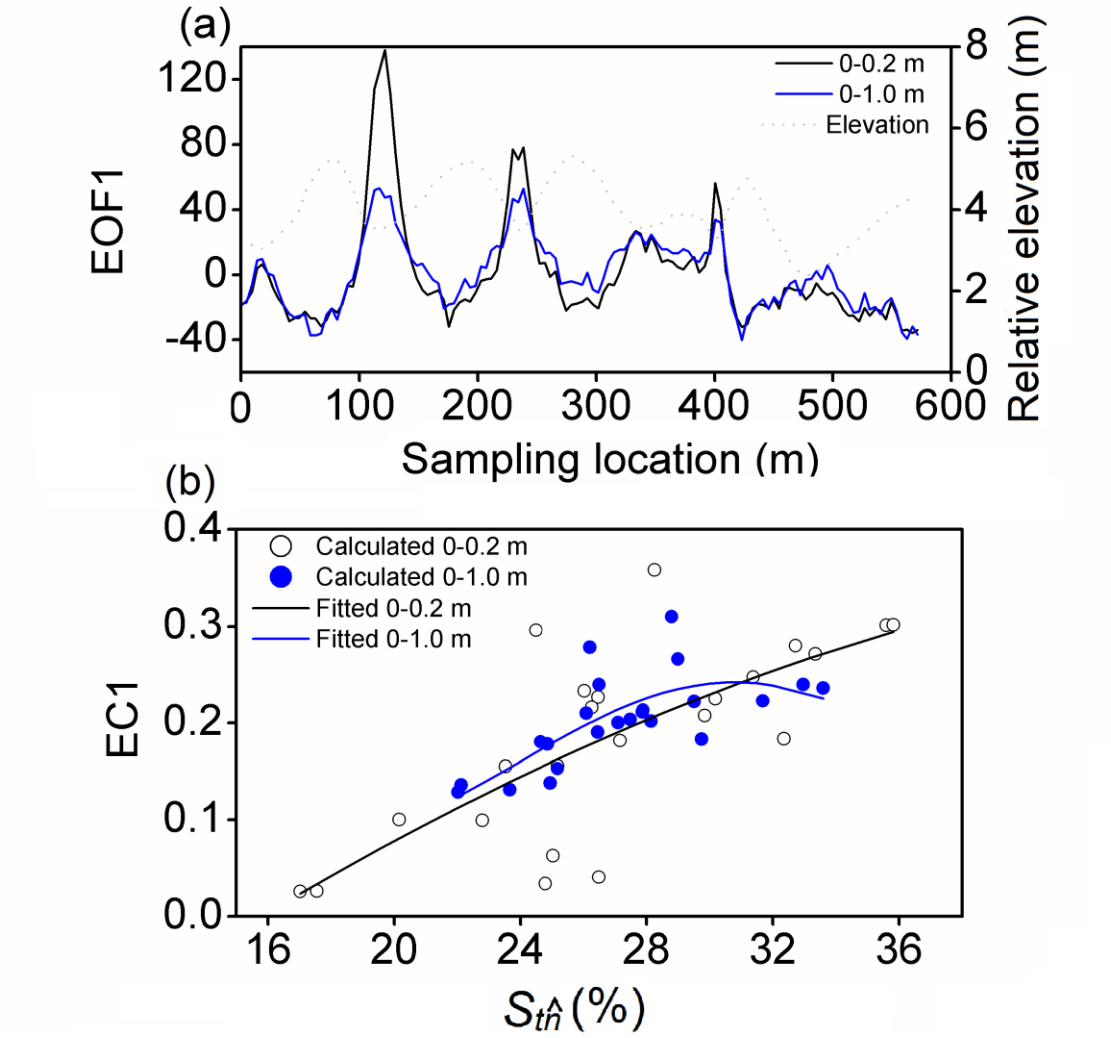

Fig. 4. (a) The EOF1 of the spatial anomaly Z_{tn} and (b) relationships of associated EC1 versus spatial mean soil water content Z_{tn} fitted by the cosine function (Eq. 4).

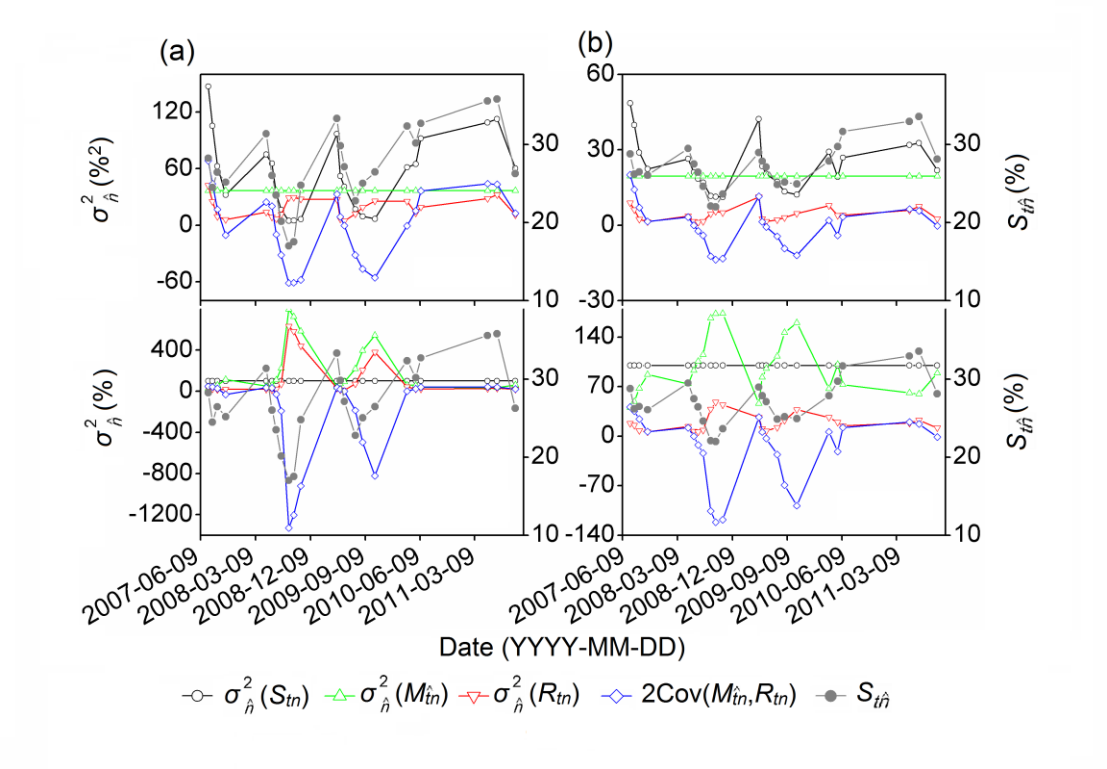

Fig. 5. Spatial variances of different components in Eq. (8) expressed in %^{2} (upper panel) and as percentage (lower panel) for (a) 0–0.2 and (b) 0–1.0 m. Spatial mean soil water content $S_{t\hat{n}}$ on each measurement day is also shown.

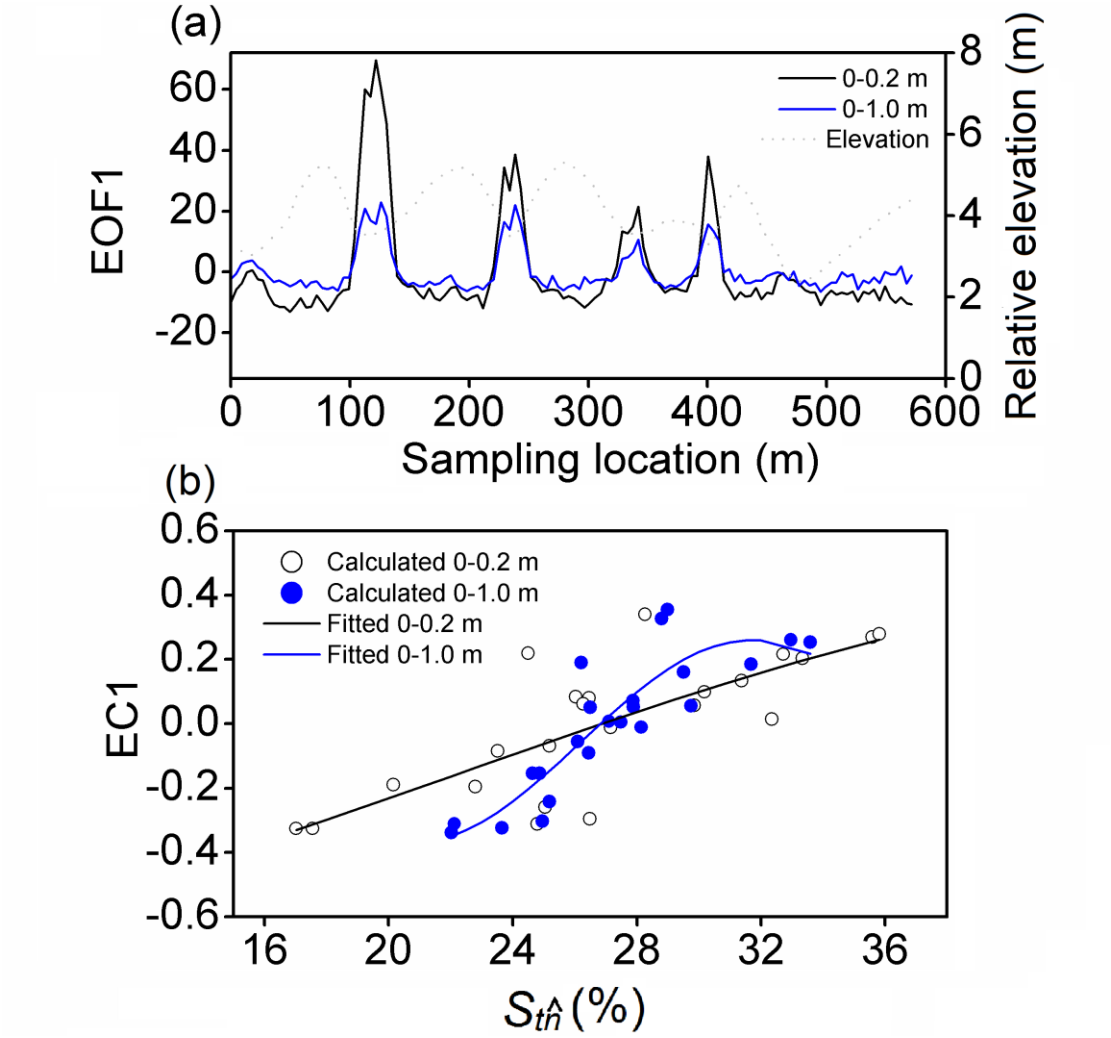

Fig. 6. (a) The EOF1 of the space-variant temporal anomaly R_{tn} and (b) relationships of associated EC1 versus spatial mean soil water content $S_{t\hat{n}}$ fitted by the cosine function (Eq. 4).

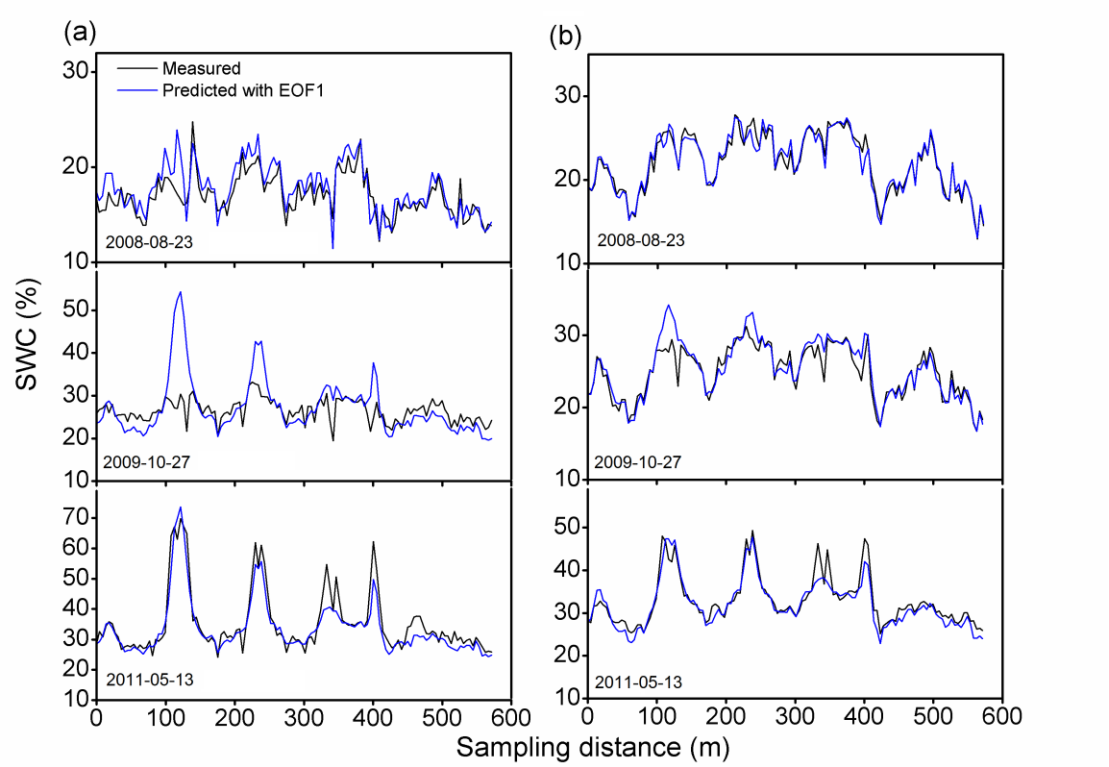

Fig. 7. Estimated soil water content (SWC) versus measured SWC for three dates at different soil water conditions (August 23, 2008, October 27, 2009, and May 13, 2011 are associated with relatively dry, medium, and wet days, respectively) using the TA model for (a) 0–0.2 and (b) 0–1.0 m.

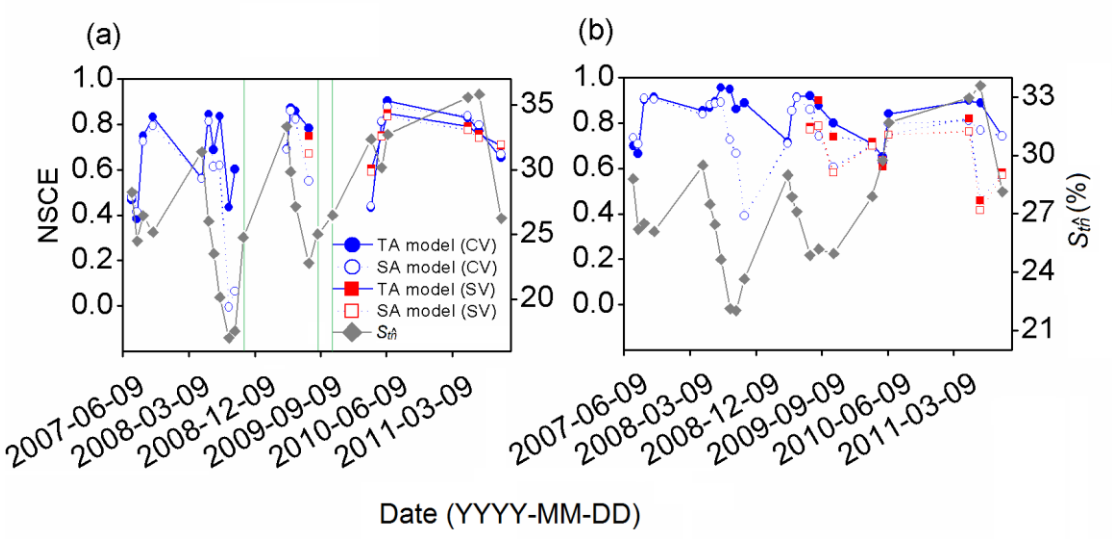

Fig. 8. The Nash-Sutcliffe coefficient of efficiency (NSCE) of soil water content estimation using the TA and SA models for (a) 0–0.2 and (b) 0–1.0 m for both cross validation (CV) and split sample validation (SV). At 0–0.2 m, three dates (October 22, 2008, August 27, 2009, and October 27, 2009) as indicated by green lines present negative NSCE values (-4.05, -1.83, and -3.81, respectively, for the CV on the three dates; -2.63 and -5.12, respectively, for the SV on the latter two dates). Spatial mean soil water content $S_{t\hat{n}}$ on each measurement day is also shown.

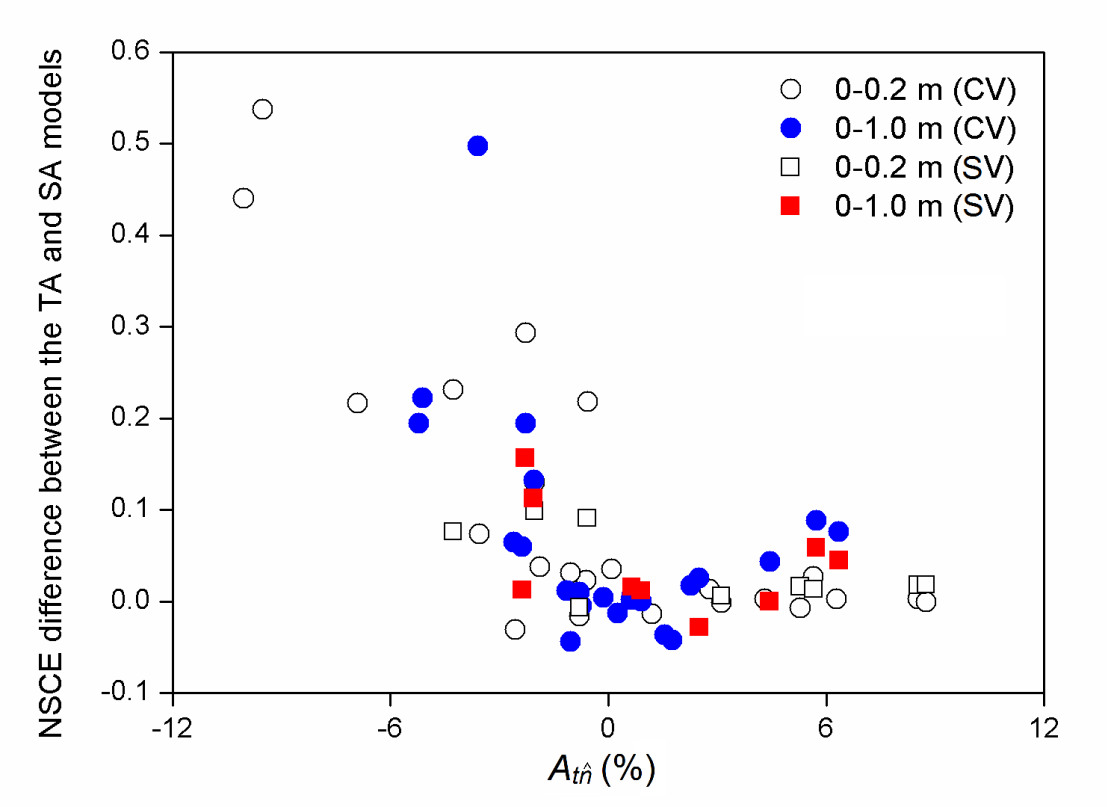

Fig. 9. Nash-Sutcliffe coefficient of efficiency (NSCE) difference between the TA and SA models in terms of soil water content estimation using both cross validation (CV) and split sample validation (SV) as a function of space-invariant temporal anomaly $A_{t\hat{n}}$ for (a) 0–0.2 and (b) 0–1.0 m.

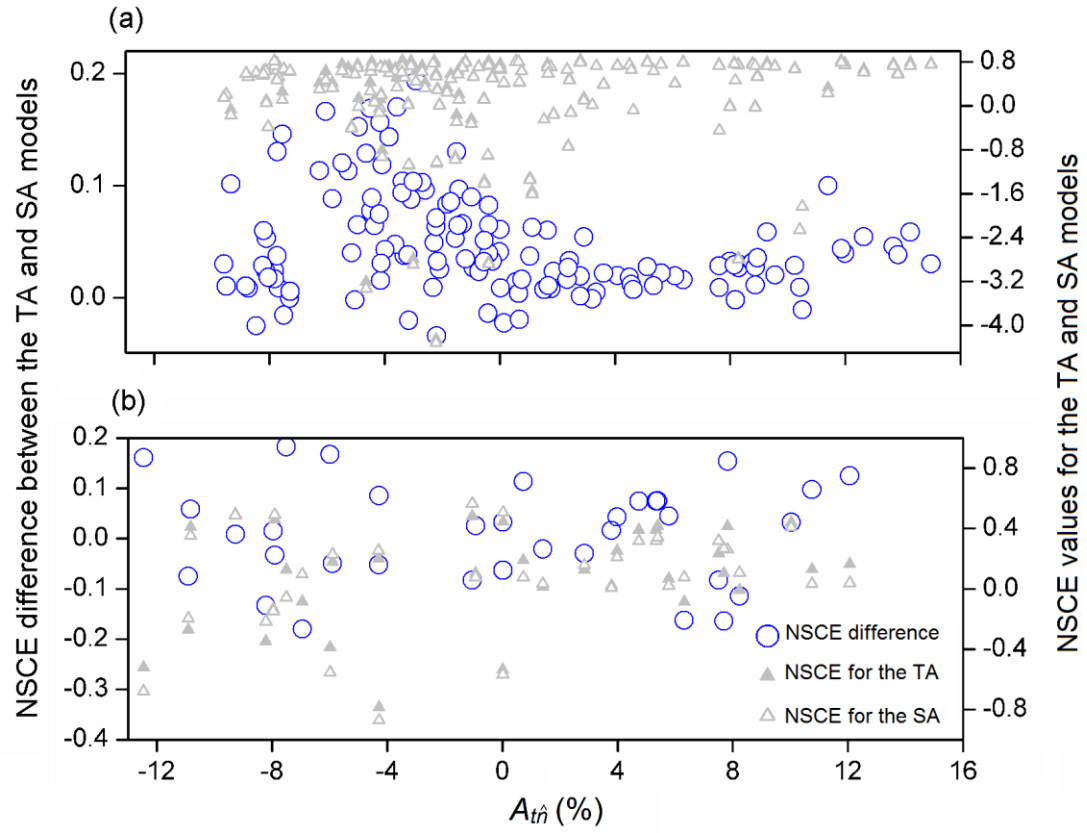

Fig. 10. Nash-Sutcliffe coefficient of efficiency (NSCE) difference between the TA and SA models in terms of soil water content estimation using cross validation as a function of space-invariant temporal anomaly $A_{t\hat{n}}$ for (a) 0–0.06 m of the Chinese Loess Plateau hillslope and (b) 0–0.15 m of the GENCAI network in Italy. The NSCE values for both models are also shown.